The 9th European Congress on Computational Methods in Applied Sciences and Engineering
ECCOMAS Congress 2024
3–7 June 2024, Lisboa, Portugal

NUMERICAL STUDY OF AN INERTIAL PARTICLE SEPARATOR EFFICIENCY UNDER THE EFFECT OF ICE ACCRETION CAUSED BY THE WATER IMPINGEMENT

LINDA BAHRAMIAN, AHMAD AMANI, JOAQUIM RIGOLA, CARLES OLIET AND CARLOS D. PÉREZ-SEGARRA

Heat and Mass Transfer Technological Center (CTTC)
Universidad Politécnica de Catalunya – Barcelona Tech (UPC)
Carrer de Colom 11, 08222 Terrassa (Barcelona), Spain
e-mail: {linda.bahramian, ahmad.amani, joaquim.rigola, carles.oliet, cdavid.perez.segarra}@upc.edu, www.cttc.upc.edu

Key words: Inertial Particle Separator, Ice Accretion, Water Impingement, Computational Fluid Dynamics, Numerical Simulation

Summary. The inertial particle separator (IPS) can face ice accretion due to the impingement of super-cooled water droplets on its inner surface. This work studies a numerical study using Computational Fluid Dynamics (CFD) for the ice accretion inside an IPS. This study is crucial in investigating the IPS performance that is affected by ice accretion. First, the numerical simulation of ice accretion for a simpler geometry, a cylinder, is validated with the experimental data. Then, the simulation of water impingement and ice accretion is studied for an IPS device. The ice profiles for different wall sections of the IPS show that ice accumulates on the bent surface of the shroud, the windward side of the hub, and the leading edge of the splitter. This accumulated ice changes the geometry of the IPS. Therefore, the separation efficiency of the IPS is expected to decrease due to the generation of ice in the way of the scavenge outlet.

1 INTRODUCTION

An Inertial particle separator (IPS) can be situated in the aircraft engine's intake to prevent the Foreign Object Debris (FOD) from entering the compressor. An IPS consists of two types of outlets: core and scavenge. The goal is to navigate particles into the scavenge outlet, which is implemented by a rapid change in flow direction. Therefore, particles separate from the core outlet by their inertia. IPS performance is measured by the separation efficiency, calculated as the mass of particles leaving the scavenge outlet over the total mass of particles leaving both outlets.

Connolly et al. [1] present experimental data for a wide range of flow path designs and test dust for an IPS device. The geometry was proposed first by Barone et al. [2]. These data can be used for validation purposes. In the work of Bahramian et al. [3], the validation of numerical simulation of an IPS device with the experimental benchmark case of Barone et al. [2] is carried out, and the separation efficiency for spherical particles is examined with the experimental data. In another work, Bahramian et al. [4] have investigated the effect of different Reynolds numbers and scavenge mass flow fractions on the separation efficiency of an IPS device through different turbulent numerical simulations.

An IPS also can face the problem of icing. In cold weather, super-cooled water droplets in the air may impact the inner surface of the IPS and cause icing, which significantly influences the IPS performance. Therefore, in order to design an effective anti-icing system, understanding the ice accretion process within the IPS is crucial. The effects of the mean droplet diameter (MVD), liquid water content (LWC), and incoming velocity on ice accretion of an IPS device of a helicopter are studied by Qiu et al. [5]. As was shown, the ice thickness on the wall surfaces changes according to the different MVDs, LWCs, and inlet velocities.

2 MATHEMATICAL MODEL

The Navier-Stokes equations represent the equations of a viscous compressible continuous fluid. To implement the Navier-Stokes equations in Large Eddy Simulation (LES) and Reynolds Averaged Navier-Stokes (RANS) turbulence methods, they can reformulated in the filtered form. In LES, the focus is on resolving the larger scale flow characteristics while the subgrid scales (SGS) are modeled. The scale separation is achieved by applying a low-pass filter to the transport equations as detailed in the work of Pope [6]. The continuity, momentum, and energy equations, which govern the flow of a compressible Newtonian fluid, are detailed in the work of Versteeg et al. [7] as follows:

$$\frac{\partial \rho}{\partial t} + \nabla \cdot (\rho \mathbf{u}) = 0 \tag{1}$$

$$\frac{\partial (\rho \mathbf{u})}{\partial t} + \nabla \cdot (\rho \mathbf{u}\mathbf{u}) = -\nabla p + \nabla \cdot (\mu \nabla \mathbf{u}) + \mathbf{S_u} \tag{2}$$

$$\frac{\partial (\rho E)}{\partial t} + \nabla \cdot (\rho \mathbf{u} H) = -\nabla \cdot (p\mathbf{u}) + \nabla \cdot (k \nabla T) + S_E \tag{3}$$

where ρ, $\mathbf{u}$ and p are the density, the velocity vector, and the pressure of the fluid. μ, $\mathbf{S_u}$ are the dynamic viscosity and the momentum source term. In the energy equation, E, H, k, T and S_E represent the total energy per unit mass, the total enthalpy per unit mass, the thermal conductivity, the temperature, and the energy source term, respectively.

As described in ANSYS Fluent, the Eulerian formulation is employed to simulate the impingement of water droplets. The general Eulerian-Eulerian model consists of the Euler or Navier-Stokes equations with additional terms accounting for the droplets:

$$\frac{\partial \alpha}{\partial t} + \overrightarrow{\nabla} . \left(\alpha \overrightarrow{V}_d \right) = 0 \tag{4}$$

$$\frac{\partial \left(\alpha \overrightarrow{V}_d \right)}{\partial t} + \overrightarrow{\nabla} \left[\alpha \overrightarrow{V}_d \otimes \overrightarrow{V}_d \right] = \frac{C_D Re_d}{24K} \alpha \left(\overrightarrow{V}_a - \overrightarrow{V}_d \right) + \alpha \left(1 - \frac{\rho_a}{\rho_d} \right) \frac{1}{Fr^2} \tag{5}$$

where α and V_d are mean-field values of the droplet concentration and velocity, respectively. C_D, Re, and K are the drag coefficient, Reynolds number, and droplet inertia parameter, respectively. The subscripts a stand for the air and d for the droplet, and the Fr represents the Froude number. The first term on the right-hand side of the momentum equation accounts for the drag force acting on droplets with a mean diameter of d. The second term accounts for buoyancy and gravity forces and is proportional to the local Froude number.

Besides continuity and momentum conservation equations for droplets, the thermal energy equation can also be considered, which enables heat exchange between droplets, airflow, and water vapor systems.

For icing, ANSYS Fluent solves a system of two partial differential equations on all solid surfaces. The first equation represents mass conservation:

$$\rho_f \left[\frac{\partial h_f}{\partial t} + \overrightarrow{\nabla}. \left(\overrightarrow{V}_f h_f \right) \right] = V_\infty LWC\beta - \dot{m}_{evap} - \dot{m}_{ice} \tag{6}$$

where h_f and V_f are the height and velocity of the water film. The three terms on the right-hand side account for the mass transfer by water droplet impingement, the mass transfer by evaporation, and ice accretion.

The second partial differential equation is the conservation of energy:

$$\begin{aligned} \rho_f \left[\frac{\partial h_f c_f T_f}{\partial t} + \overrightarrow{\nabla}. \left(\overrightarrow{V}_f h_f c_f T_f \right) \right] = & \left(e_d + \frac{1}{2} \overrightarrow{V}_d^{\,2} \right) V_\infty LWC\beta - \dot{m}_{evap} \left(L_{evap} \right) \\ & + \dot{m}_{ice} \left(L_{fus} - c_{ice} T_{ice} \right) - c_h \left(T_f - T_{rec} \right) + \sigma\varepsilon \left(T_\infty^4 - T_f^4 \right) + Q_{anti-icing} \end{aligned} \tag{7}$$

where the first three terms represent the energy transfer by the impinging super-cooled water droplets, evaporation, and ice accretion, and the last three terms correspond, respectively, to the radiative, convective, and 1D conductive heat fluxes that could be applied by an anti-icing heater device.

The coefficients $\rho_f, c_f, L_{evap}, c_{ice}, L_{fus}, \sigma, \varepsilon$ are physical properties of water and ice that are adjustable in the user interface. The reference conditions T_∞, V_∞, LWC are airflow and droplet parameters of the freestream.

Droplet simulation provides local values of the collection efficiency β, droplet energy e_d, and droplet impact velocity V_d. The local water collection efficiency can be determined using:

$$\beta = -\frac{\alpha \overrightarrow{V_d}. \overrightarrow{n}}{(LWC_\infty) U_\infty} \tag{8}$$

where α is the local liquid water content; $\overrightarrow{V_d}$ and $\overrightarrow{n}$ are the droplet impact velocity and the surface normal vector; and LWC_∞ and U_∞ are the freestream liquid water content and velocity of the droplets, respectively.

The evaporative mass flux m_{evap} is recovered from the convective heat transfer coefficient using a parametric model. $Q_{anti-icing}$ is the anti-icing heat flux for wet air calculations, h_f and T_f are the film thickness and the equilibrium temperature at the air/water film/ice/wall interface, and m_{ice} is the instantaneous mass accumulation of ice.

3 RESULTS AND DISCUSSIONS

In this section, first, a validation for water impingement and ice accretion is implemented, and in the following, the ice accretion is studied in an IPS device. For water impingement, the Eulerian-Eulerian approach is implemented. The numerical simulations were carried out using the turbulence method of RANS by the Spalart-Allmaras model in ANSYS Fluent.

3.1 Ice accretion validation

For the validation purpose, a simple case of a cylinder with a diameter of $38.1mm$ is selected. The experimental results for this case are presented by Koss [8]. A mesh sensitivity analysis is performed, and as shown in figure 1, a structured mesh of around 200K control volumes (CVs) is implemented. The mesh is refined adequately around the cylinder to maintain better precision in the results. The Reynolds number of inlet flow is in the range of 2 million. The ice condition is listed in the table 1.

Table 1: Simulation conditions for ice accretion on the cylinder

$U_\infty(m/s)$	$T(K)$	$LWC(g/m^3)$	$MVD\ (\mu m)$	$t(s)$
30	269.15	0.4	50	600

Figure 2 shows the water collection coefficient on the cylinder. Due to the high inertia of the water droplets, it is challenging to change their trajectory, resulting in most droplets impacting the leading edge of the cylinder, where β becomes significantly large. Figure 3 shows the ice profile comparison of the numerical simulation with the experimental data, which presents a good agreement between them. The results demonstrate the accuracy and capability of the current model, which can be implemented for more complex geometry.

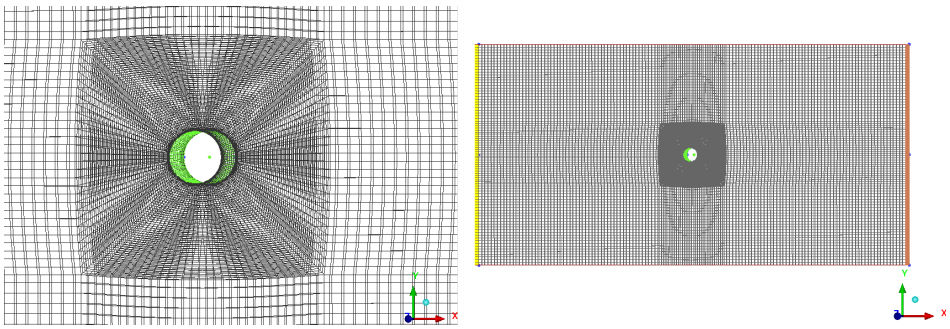

Figure 1: Structured mesh used for the simulation of ice accretion on the cylinder.

3.2 IPS water impingement and ice accretion

For IPS, the OSG-1 geometry of Barone et al. [2] with the scavenge mass flow fraction of 0.16 is selected. The width of the geometry is set to $0.2m$. Figure 4 represents a general geometric model of an IPS, showing the inlet, scavenge and core outlets, and three different walls: shroud, hub, and splitter. As shown in figure 5, a structured mesh refined especially close to the walls and in the curvatures is used. The simulation condition is listed in table 2. The Reynolds number of the IPS based on the characteristic length of $0.068m$ is around 500K. The inlet pressure is set to atmospheric pressure (101.325 kPa), while the mass flow rates are specified for both the core and scavenge outlets.

Figure 6 shows the local water collection coefficient distribution, β, for three different walls of the IPS: shroud, hub, and splitter. The reason behind the water accumulation in the bent

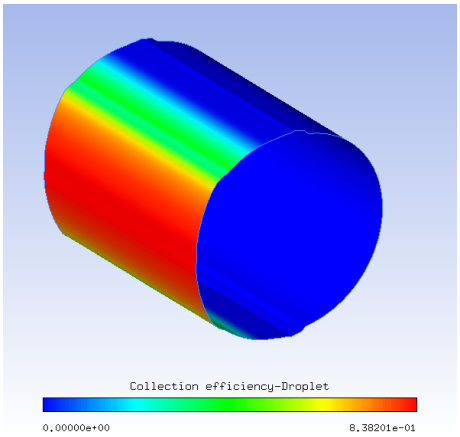

Figure 2: Contour of the water collection coefficient on the cylinder.

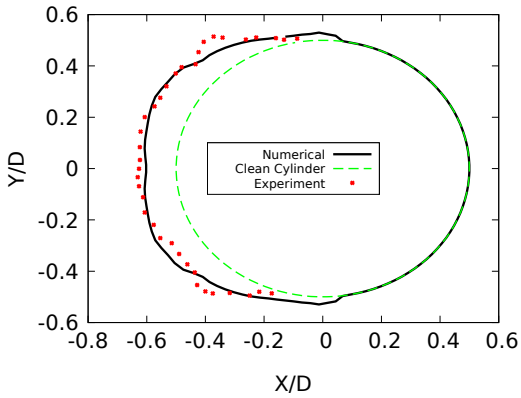

Figure 3: Comparison of the accumulated ice profile with the experimental data.

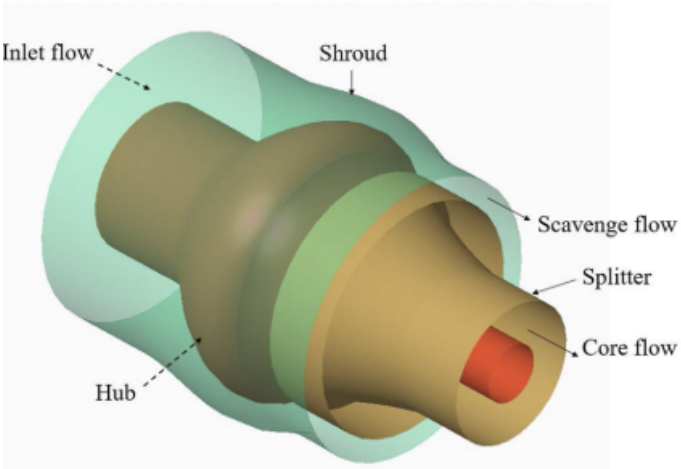

Figure 4: Geometric model of the IPS [5].

Table 2: Simulation conditions for ice accretion on the IPS

$U_\infty(m/s)$	$T(K)$	$LWC(g/m^3)$	$MVD\ (\mu m)$	$t(s)$
90	253.15	2	20	360

surface of the shroud is as super-cooled water droplets enter the IPS, they gradually accelerate to their peak velocity before passing through the throat, where the curvature is most pronounced. Due to their high inertia, these high-speed droplets cannot change direction as quickly as the surrounding airflow. Consequently, they deviate from the air stream and impact the wall independently. As a result, the IPS effectively reduces the amount of water entering the core flow path by capturing it on the inner walls.

The ice profiles for these three walls of the IPS are shown in figure 7 within an icing time of 6 min. The ice generated on these surfaces will change the internal geometry of the IPS, and as

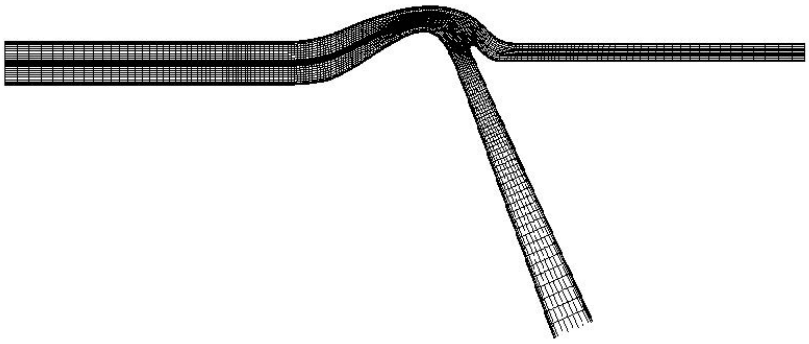

Figure 5: Structured mesh generated for the simulation of the IPS.

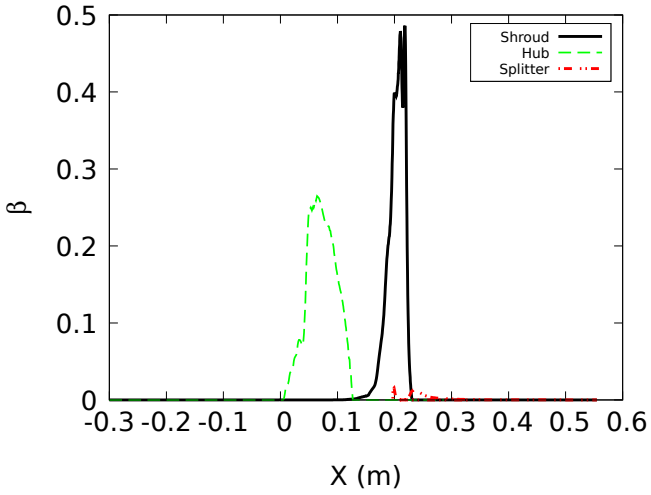

Figure 6: Local water collection coefficient distribution on different walls of the IPS.

a result, the ability of the IPS to navigate the FOD to the scavenge outlet will change. The wall collision coefficient will change accordingly as the ice material differs from the walls. Due to the accumulated ice in the shroud, the efficiency of the IPS is expected to decrease. However, the numerical value of separation efficiency is under implementation for a comprehensive conclusion of this phenomenon.

4 CONCLUSIONS

This work investigated the numerical simulation of water impingement and ice accretion inside an IPS device. The 3D RANS turbulence model is implemented through ANSYS Fluent software for the numerical simulation. The benchmark case of Koss [8] was chosen as a validation test case of a cylinder for the ice accretion numerical simulation. Numerical results on the ice profile of the cylinder benchmark case were in good agreement with the experimental data. The results of the water impingement and the ice accretion of the IPS indicate the critical area to consider for the separation efficiency. As the accumulated ice in the shroud wall is narrowing the scavenge outlet entrance, it prevents the particles from erasing correctly from the scavenge outlet, and as a result, the separation efficiency of the IPS will decrease. The effect of LWC, MVD, incoming

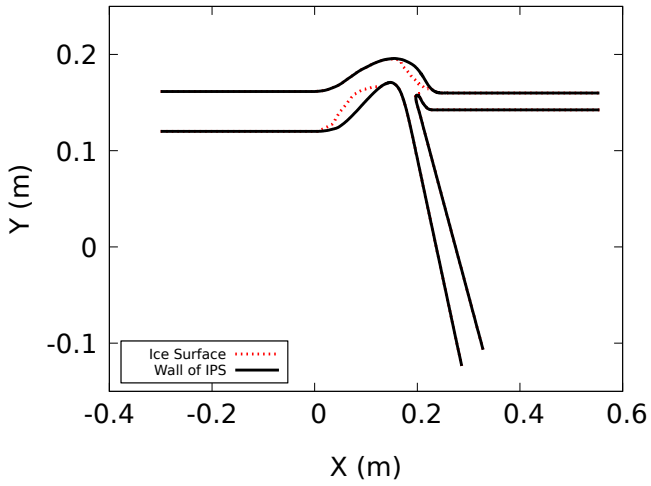

Figure 7: 2D ice shape on different walls of the IPS.

velocity, and temperature on ice accretion inside the IPS is under implementation. Further analyses of the effect of ice accretion on the airflow field and separation efficiency value of the IPS will be investigated.

ACKNOWLEDGEMENTS

Linda Bahramian acknowledges the financial support from the Secretariat of Universities and Research of the Generalitat de Catalunya and the European Social Fund, FI AGAUR Grant (2019 FI_B 01205), and the UPC-Santander Grant. Carles Oliet, as a Serra Húnter associate professor, acknowledges the Catalan Government for the support through this Programme.

Horizon 2020
European Union Funding
for Research & Innovation

Clean Sky 2
JOINT UNDERTAKING

This project has received funding from the Clean Sky 2 Joint Undertaking under the European Union's Horizon 2020 research and innovation programme under grant agreement No 821352 (ANTIFOD project).
Disclaimer: The contents presented in this article reflect only the author's point of view: Clean Sky JU are not responsible for any use that may be made of the information it contains.

REFERENCES

[1] Connolly B.J., Loth E., and Smith C.F. 2022. "Unsteady separated flows in an S-Duct and a bifurcating duct." J. Aircr. 59(1): 47-57. https://doi.org/10.2514/1.C036383

[2] Barone D., Loth E., and Snyder P. 2017. "Influence of particle size on inertial particle separator efficiency." Powder Technol. 318: 177-85. https://doi.org/10.1016/j.powtec.2017.04.044

[3] Bahramian, L., Amani, A., Rigola, J., Oliet, C., and Pérez-Segarra, C.D. 2024, May. "On the validation of numerical simulation with experimental results on compressible turbulent flow in an inertial particle separator device." In Journal of Physics: Conference Series, vol. 2766, no. 1: 012113. IOP Publishing. http://doi.org/10.1088/1742-6596/2766/1/012113

[4] Bahramian, L., Amani, A., Rigola, J., Oliet, C., and Pérez-Segarra, C.D. 2023. "A numerical study on turbulent flow in an inertial particle separator device." 10th Int. Symp. on Turbulence, Heat and Mass Transfer (Rome) ICHMT Digital Library Online (New York: Begel House Inc.) http://doi.org/10.1615/ICHMT.THMT-23.830

[5] Qiu, C., Chen, N., Hu, Y., Wang, B., and Hu, S. 2022. "Numerical study of ice accretion inside an inertial particle separator." AIP Advances 12, no. 5. https://doi.org/10.1063/5.0093145

[6] Pope S.B. 2001. Turbulent Flows, Measurement Science and Technology vol 12 no. 11: 2020-1

[7] Versteeg H.K., and Malalasekera W. 2007. An Introduction to Computational Fluid Dynamics: the Finite Volume Method, (Pearson education)

[8] Koss, H.H., Gjelstrup, H., and Georgakis, C.T. 2012. "Experimental study of ice accretion on circular cylinders at moderate low temperatures." Journal of Wind Engineering and Industrial Aerodynamics, 104: 540-546. https://doi.org/10.1016/j.jweia.2012.03.024